# Fabrication and evaluation of an attapulgite membrane as the filter for recycling blowdown water from industrial boilers

Baomin Fan, Hua Hao, Anru Guo and Ruping Yang

## ABSTRACT

Continuous blowdown water (CBW) from industrial boilers is of great quantity and energy, and therefore worth recycling. According to the data from a long period of monitoring, carbonate and sulfate were documented as the main contaminants in CBW. Herein, an attapulgite (ATP) membrane was prepared on a macroporous $Al_2O_3$ support through solid state sintering. The prepared membrane (attapulgite membrane (ATM)) was characterized by mercury porosimetry, scanning electron microscope, X-ray diffraction, and permselectivity analysis in dead-end mode. The optimal sintering temperature was 800 °C based on the morphology of the sintered active layer and its adhesive strength with support. The active layer exhibited a pore size distribution concentrated on 12.7 nm with a thickness of about 80 μm. In addition, crystal structures of ATP were retained in powder form after sintering. ATM obtained a pure water permeability of 1,411.87 L $m^{-2}$ $h^{-1}$ $MPa^{-1}$ with the effective retention of carbonate and sulfate through electrical-related interactions. Several ATM filters were also developed and mounted on the boiler blowdown pipe, which had a high rejection rate of alkalinity and dissolved solids in CBW. The volume of wastewater emitted from the low-pressure boiler was reduced, since the filtrate could be recycled as part of the make-up water.

**Key words** | attapulgite, ceramic membrane, continuous blowdown water, industrial boiler, make-up water

**Baomin Fan** (corresponding author)
Department of Materials Science and Engineering,
Beijing Technology and Business University,
Beijing 100048,
China
E-mail: *fanbaomin@btbu.edu.cn*

**Hua Hao**
Chinese Academy of Sciences,
Institute of Chemistry,
Beijing 100190,
China

**Anru Guo**
**Ruping Yang**
Aerospace Research Institute of Materials and Processing Technology,
China Aerospace Science and Technology Corporation,
Beijing 100076,
China

## NOMENCLATURE

| | |
|---|---|
| $A$ | effective filtering area, $m^2$ |
| $J$ | pure water permeability, L $m^{-2}$ $h^{-1}$ |
| $m_1$ | mass of the dried membrane, kg |
| $m_2$ | mass of the solid-saturated membrane, kg |
| $m_3$ | mass of the water-saturated membrane, kg |
| $p$ | imposed pressure, MPa |
| $Q_{CBW}$ | volume of CBW, $m^3$ $h^{-1}$ |
| $Q_S$ | volume of steam product, $m^3$ $h^{-1}$ |
| $q$ | porosity of the membrane, % |
| $R$ | ion rejection rate, % |
| $r$ | pore size of the membrane, nm |
| $t$ | filtering time, h |
| $V$ | volume of the filtrate, L |

### Greek letters

| | |
|---|---|
| $\gamma$ | surface tension of mercury, 0.48 N/m |
| $\eta$ | blowdown rate of the industrial boiler, % |
| $\theta$ | contact angle between the membrane and solution, degree |
| $\rho_0$ | ion concentrations in the feed solution, mg/L |
| $\rho_f$ | ion concentrations in the filtrate, mg/L |

### Subscripts

| | |
|---|---|
| CBW | continuous blowdown water |
| f | feed |
| S | steam |

doi: 10.2166/wrd.2016.148

## INTRODUCTION

Boilers are used as the power source in most process industries (Luo *et al.* 2012). Thus, they are usually regarded as the 'heart' of industries. Based on the working principle of the steam engine, water can be boiled and transferred to pressurized steam by burning fossil fuels. The pressurized steam drives the related mechanical parts to achieve energy conversion. Boilers are the device for water reserve and steam production, which are usually treated as the power source in most process industries. Thereby, the intrinsic energy contained in fossil fuels can be converted to other forms of counterparts (electrical energy, heat, kinetic energy, etc.) for human utilization through the assistance of boilers. With accumulated operating experience, periodical and continuous blowdown have become the necessary procedures to prevent corrosion and deposition, and for secure operations. Insufficient blowdown will not only make the boiler water unqualified, but also threatens the safety of operation. Periodical and continuous blowdown are necessary procedures during boiler operation. Large quantities of water have to be emitted from the boiler body, resulting in high waste production. In order to maintain the water/vapor balance, equal amounts of fresh water to wastewater should be introduced into the boiler system. Another aspect deserving attention is that the wastewater emitted from the boiler contains lots of energy, which will be lost during the blowdown procedure.

In summary, we make the conclusion that industrial boilers are units of energy intensive, water consuming, and high waste production.

In general, boilers with lower pressure usually have a higher blowdown rate. According to the relevant reports in China (Li *et al.* 2009; Wei *et al.* 2013), the blowdown rate of low-pressure boilers ($\leq$2.45 MPa) could reach 10% or even higher. In addition, boilers with different rated pressures have different types of working processes and components of contaminants in continuous blowdown water (CBW). (Li *et al.* 2009). For example, phosphate is the dominant pollutant in the CBW of medium-pressure boilers (~3.82 MPa); meanwhile, sulfate ($SO_4^{2-}$), alkalinity ($CO_3^{2-}$, $HCO_3^-$ and $OH^-$) and metal cations ($Na^+$) make up the main pollutants in the CBW of low-pressure boilers (Saidur 2011; Wei *et al.* 2013). Discharging CBW without proper treatment will undoubtedly pose an eco-toxicological threat to the organisms in receiving water bodies and soil. Besides, blowdown volume, especially from low-pressure boilers, is an obvious target for saving fresh or treated water, and chemical treatment.

One of the most efficient ways to treat wastewater is membrane technology, which is an effective and reliable method for the combined removal of a broad range of pollutants (Rana & Matsuura 2010). Taking into account the different separating mechanisms, rejection processes and pore size distributions, membranes can be classified as different types: microfiltration, ultrafiltration, nanofiltration and so forth (Shirazi *et al.* 2013). Most nano-scale membranes are usually made from polymers for high separation efficiency (Agana *et al.* 2013). Polymeric membranes can separate aqueous mixtures containing strong electrolytes and/or uncharged solutes through the effects of electrostatic interactions (Luo & Wan 2013). Recently, ceramic membranes have gained increasing popularity for water treatment due to many inherent advantages over their polymeric counterparts such as high mechanical and chemical stability, and enhanced hydrophilicity (Chang *et al.* 2014). However, ceramic membranes, which could interact with charged species through electrical-related effects, are usually made from amphoteric material ($Al_2O_3$, $TiO_2$ or $ZrO_2$) by a sol-gel method (Chang *et al.* 2014). Moreover, organic solutions and nucleating agents are necessities during preparation for the integrity of membranes. Therefore, it is desired to develop a ceramic membrane with electrokinetic properties based on clay minerals via simple sintering.

Attapulgite (ATP) is one of the cost-effective natural minerals, which can be surface mined in eastern and southern parts of China (Deng *et al.* 2013). Because of its permanent negative surface charge and non-swelling properties, ATP powder has become an attractive material in water treatment with different degrees of success (Shi *et al.* 2013; Yin & Kong 2014; Liu *et al.* 2015). Adsorption is a widely accepted way for ATP to purify the discharged effluent. Unfortunately, alkali metal ions, which are inevitable in industrial wastewater, can adversely affect the adsorption capacity of ATP (Shi *et al.* 2013). Thus, an increasing number of studies have concentrated on the modification

of ATP powder for enhanced contaminant retention and retarded contaminant migration. For instance, natural ATP was activated by dilute hydrochloric acid and further functionalized by ethylenediamine for lead removal in water (Deng *et al.* 2013); a porous material based on polyurethane and ATP could be considered as an efficient adsorbent for dyeing wastewater treatment (Dong *et al.* 2013). A survey of the literature reveals that little attention has been paid to the preparation of an active membrane layer made of ATP for purifying saline wastewater.

The present study will of necessity encapsulate the preparation of an attapulgite membrane (ATM) on macroporous $Al_2O_3$ support through solid state sintering. The performance of the ATM is evaluated by laboratory-scale experiments in dead-end mode. Several membrane filters were developed based on ATM, and these were applied to treat the CBW from an industrial boiler.

## MATERIALS AND METHODS

### Chemicals and reagents

ATP was purchased from the Chunqiu Ceramic Workshop (Zibo, China). X-ray fluorescence (Shimadzu, Japan) was used to determine the chemical composition of the ATP, which is summarized in Table 1. Commercially available $Al_2O_3$ supports were from Fengxi Porcelain Factory (Chaozhou, China). The specific parameters of the supports are listed in Table 2. Analytical grade hydroxyethyl cellulose, $Na_2CO_3$, $Na_2SO_4$, NaOH, NaCl and hydrochloric acid were obtained from Beijing Chemical Works (Beijing, China) and used as received. Except where otherwise stated, all the solutions mentioned in this study were prepared using deionized (DI) water with a conductivity of 7.6 μS/cm, which was prepared through an HA-10LB style ultra-pure water system of Berclean Company (Chongqing, China) and used at its native pH (6.0 ± 0.2).

### Sampling of CBW

Online monitoring of practical CBW discharged from a local WNS20–1.57YQ style boiler (Xinzheng Cigarette Factory, China) was carried out for 8 months. The samples were stored through the methods described in GB/T 6907-2005 for experiments in the laboratory (Standard GB/T 6907-2005). The characteristics of CBW are recorded in Table 3, which were determined according to the methods described by the American Public Health Association (APHA/AWWA/WEF 1998).

### Preparation of ATP membrane

Before the coating procedure, pre-treatment of $Al_2O_3$ supports was carried out by grinding with emery paper of grade number 800, 1,000, 1,200, 1,600 and 2,000, rinsing, ultrasonic cleaning in DI water under 40 kHz for 15 min, and oven-drying at 80 °C.

The ATP powder was mixed with hydroxyethyl cellulose and water under vigorous stirring until a stable turbid solution (ATP, 8 wt.%) was harvested. A Petri dish was utilized to hold the ATP suspension. One side of the $Al_2O_3$ support was then dipped vertically into the suspension for 10 s and a wet ATP coating layer formed because of the capillary effect. All the coated substrates were transferred into a desiccator over silica gel at room temperature (27 °C, overnight) for natural drying. Afterwards, they were oven-dried at 90 °C to remove the residual moisture, and then sintered at the desired temperatures for 3 h with a heating rate of 1 °C $min^{-1}$ in a SX2-2.5-12 style muffle furnace (Beijing Furnace Factory, China). After natural cooling, each as-prepared membrane was carefully collected for subsequent tests.

### Characterization

According to the method described in GB/T 9286-1998 (Standard GB/T 9286-1998), the adhesive strength level

**Table 1** | Compositions of natural clay. LOI is loss on ignition

| Material | Chemical composition (wt.%) | | | | | | | | | |
|---|---|---|---|---|---|---|---|---|---|---|
| ATP | $SiO_2$ | MgO | $Al_2O_3$ | $Fe_2O_3$ | $TiO_2$ | $Na_2O$ | $SO_3$ | $P_2O_5$ | MnO | LOI |
| | 55.13 | 21.57 | 17.41 | 3.75 | 1.43 | 0.31 | 0.10 | 0.05 | 0.02 | 0.23 |

**Table 2** | Main parameters and hydraulic performance of purchased $Al_2O_3$

| Item | Unit | Values |
|---|---|---|
| Diameter | mm | 90 |
| Thickness | mm | 4 |
| Porosity | % | 37.32 |
| Pure water flux | L $m^{-2}$ $h^{-1}$ | 8,341.67 under 0.1 MPa |

**Table 3** | Water quality of CBW from the WNS20-1.57YQ style boiler (August 2013–April 2014)

| Parameters | Unit | Mean values |
|---|---|---|
| pH (25 °C) | | 11.51 |
| Calcium ($Ca^{2+}$) | mg $L^{-1}$ | Not detected |
| Magnesium ($Mg^{2+}$) | mg $L^{-1}$ | Not detected |
| Sodium ($Na^{+}$) | mg $L^{-1}$ | 1,283.18 |
| Chloride ($Cl^{-}$) | mg $L^{-1}$ | 6.07 |
| Sulfate ($SO_4^{2-}$) | mg $L^{-1}$ | 405.63 |
| Carbonate ($CO_3^{2-}$) | mg $L^{-1}$ | 1,415.08 |
| Suspended solids | mg $L^{-1}$ | Not detected |
| Temperature | °C | 109 |
| Pressure | MPa | 0.14 |

between the ATP active layer and $Al_2O_3$ support was determined. The strength contains six levels: the lower the level, the higher the strength. The porosity ($q$, %) of the ATM was determined based on the Archimedes drainage method (Jakobs & Koros 1997):

$$q = \frac{m_2 - m_1}{m_2 - m_3} \times 100\% \quad (1)$$

where $m_1$, $m_2$ and $m_3$ are the mass of the dried, solid-saturated and water-saturated membranes, respectively, in kg. It is noteworthy that the active layer cannot be totally detached from the support; thereby, the result of the ATP active layer should be subtracted from the contribution of the background ($Al_2O_3$ support).

The pore size distribution was measured through an AutoPore IV9500 style mercury porosimeter (Micromeritics, USA) based on Washburn's equation (Chibowski & Holysz 1992):

$$r = \frac{-2\gamma \cos\theta}{p} \quad (2)$$

where $r$ is the pore size, nm; $\theta$ is the contact angle between the membrane and solution, degrees; $\gamma$ is the surface tension of mercury (0.48 N/m) and $p$ is the imposed pressure, MPa.

The surface morphology was observed through an FEI Quanta FEG 250 style field emission environmental electron microscope; before scanning, the samples were gold coated through a sputtering device. Crystalline properties of the as-prepared samples were characterized through a D/max2500VB 2 + /PCX style X-ray diffractometry (XRD, Rigaku Corporation, Japan). Zeta potentials of the membrane were determined based on streaming potential analysis and the Helmholtz–Smoluchowski model (Rodemann & Staude 1995); the pHs of influent solutions were adjusted to a desired value by adding negligible volumes of 0.1 M HCl or 0.1 M NaOH solution.

## Laboratory-scale filtration experiment

The filtration experiments were conducted using a stirred cell with a volume of 400 mL described in our previous study (Wei *et al.* 2013). The DI water or model solutions were pressurized through the flat membrane with the help of a nitrogen cylinder. Pressures were monitored by a manometer of the treatment chamber.

Prior to filtration, a compaction procedure was performed as follows: the fresh membrane was immersed in DI water for at least 2 h and then was conditioned by filtering DI water under 0.6 MPa for 1 h. The membrane was also subjected to equilibrate in the test solution for a while before each experimental run. The pure water permeability ($J$, L $m^{-2}$ $h^{-1}$) could be mathematically described by Equation (3):

$$J = \frac{V}{A \cdot t} \quad (3)$$

where $A$ denotes the effective filtering area, $m^2$; $t$ denotes the filtering time, h; and $V$ is the volume of filtrate, L.

The ion rejection performance ($R$, %) of the ATM was evaluated according to Equation (4):

$$R = \frac{\rho_0 - \rho_f}{\rho_0} \times 100\% \quad (4)$$

where $\rho_0$ and $\rho_f$ represent the ion concentrations in the feed solution and filtrate, respectively, mg/L. All the laboratory-scale tests were conducted at room temperature (27 °C), and run in duplicate or more to check the reproducibility.

### Field test

Several filters were developed based on the ATM, which were mounted on the continuous blowdown pipe of a WNS20-1.57YQ style boiler. The working pressure of this boiler was 1.1 ± 0.1 MPa with a saturated steam temperature of 183 ± 1 °C. The water quality of the CBW before and after treatment was recorded from an online monitoring device. The blowdown rate ($\eta$, %) was evaluated according to Equation (5):

$$\eta = \frac{Q_{CBW}}{Q_S} \quad (5)$$

where $Q_{CBW}$ and $Q_S$ represent the volume of CBW and steam product, respectively, $m^3\ h^{-1}$. In normal operation, the average amount of steam product ($Q_S$) is about 18.70 $m^3\ h^{-1}$.

## RESULTS AND DISCUSSION

### Determination of optimum sintering temperature

Ceramic coating on an $Al_2O_3$ support is a double sintering process. The connection between the active layer and support will be not tight enough under relatively low sintering temperature; however, surface flaws, such as cracks, will appear at excessively high temperatures, especially for the asymmetric membrane. To this end, it is worth determining the optimum sintering temperature for the ATP active layer.

Figure 1 shows the adhesive strength levels between the active layer and support under different sintering temperatures. In relation to asymmetric membranes, the adhesive strength between the active layer and support should be at least Grade 3 (Standard GB/T 9286-1998). From Figure 1, the adhesive strength shows an enhanced tendency with elevated temperature, and reaches Grade 3 at 800 and 850 °C, rising to Grade 2 at 900 and 950 °C. Therefore, the sintering temperature should be over 800 °C to achieve the specification requirement.

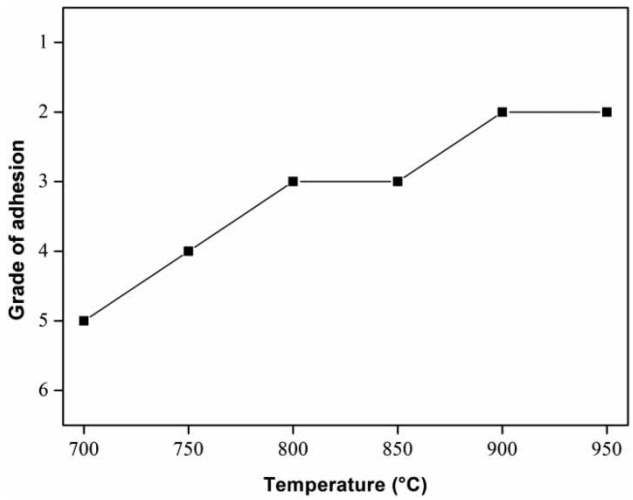


**Figure 1** | Adhesive strength levels between the ATP active layer and the $Al_2O_3$ support under different sintering temperatures.

Moreover, porosity is another key parameter for ceramic membranes, since it can affect the hydraulic performance during the separation and purification process. To a certain degree, the decisive factor affecting porosity is the sintering temperature. Figure 2 shows the surface morphology and porosities of the as-prepared membranes at different sintering temperatures. It can be observed that the pores of the ATM seem to be dying out as the temperature increases. In addition, Figure 2(d) reveals that the porosity declines steadily with increasing temperature: the determined values are 36.75%, 27.83% and 20.04% at sintering temperatures of 800 °C, 850 °C and 900 °C, respectively. The decreasing tendency can be attributed to the melting of raw material under relatively high temperature, which is conducive to the formation of liquidoid. Although the surface adhesive strength is enhanced (Figure 1) because of the penetration of liquidoid into the membrane pores, the crystal structure of the ATP might be impaired for the fusion of adjacent mineral particles. This subsequently

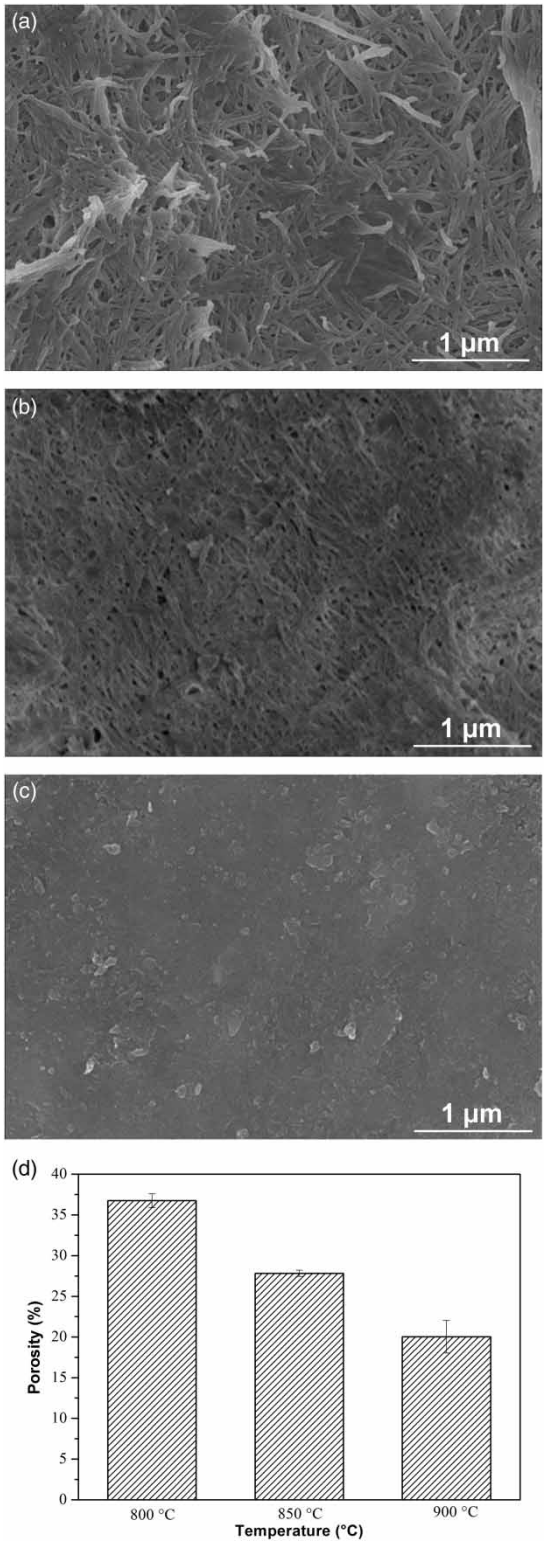


**Figure 2** | Surface morphology (sintering temperature: (a) 800 °C; (b) 850 °C; (c) 900 °C) and porosity (d) of ATM.

leads to severe blockage of pores, generating a low porosity. In general, the porosity of ceramics is usually more than 30% (Maarten Biesheuvel & Verweij 1999); therefore, from the standpoints of adhesive strength and porosity, the sintering temperature for the ATM is selected at 800 °C in this work.

## Characterization of ATM

ATP powder has unique crystal characteristics, which enable it to exhibit permanent negative charges on the particle surface (Huang *et al.* 2007). Therefore, it is of value to analyze the crystal information of the ATP before and after sintering through XRD technology, and the results are shown in Figure 3. As can be observed, both ATP powder and the as-prepared membrane are composed of $SiO_2$, $Mg_2SiO_4$, and a small content of $Al_{4.5}FeSi$ as well as $Al_8Si_6Mg_3Fe$. The characteristic $d$ spacing of 10.64, 4.48, 4.25, and 3.34 Å confirms the sample used in this work is ATP (Huang *et al.* 2007). After sintering, the peak intensity of $d$ spacing at 10.64 Å lessens noticeably; conversely, that of $d$ spacing at 3.34 Å enhances sharply. This is evidence that the membrane forming process only changes the

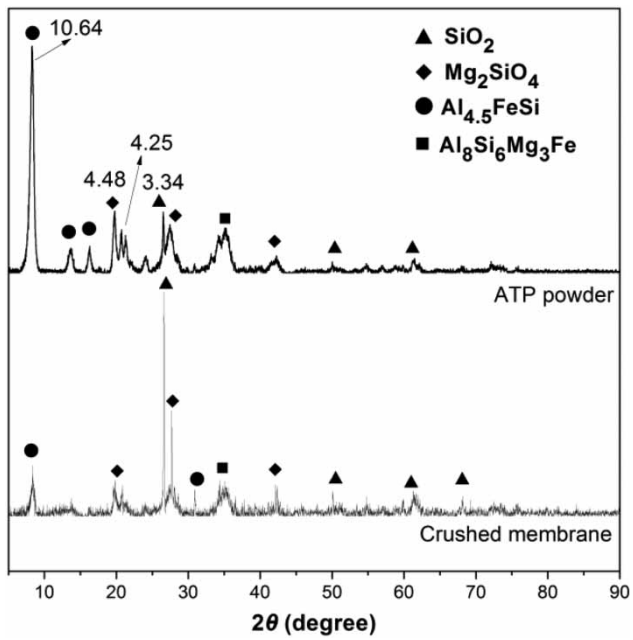


**Figure 3** | XRD patterns of ATP before and after sintering at 800 °C.

crystallinity of certain phases rather than the charge-related parameters, such as the crystal lattice, lattice parameter and crystallite dimensions. Therefore, it is reasonable to assume that the ATM would keep a charge property similar to that of ATP powder.

Further study on the pore size distribution of the $Al_2O_3$ support and ATM is shown in Figure 4. It can be seen that the pore size of the support ranges from 7,178.85 to 8,239.74 nm; with respect to the active layer, the pore sizes are concentrated on 13.39 nm. Combining Washburn's theory (Chibowski & Holysz 1992) and Equation (2), the mean pore size of the active layer is observed to be 12.7 nm. Therefore, the much more open morphology of the support compared with that of the ATP layer is easily visible. This result is directly supported by SEM images shown in Figure 5(a) and 5(b). It is worth mentioning that the active layer is formed by irregular accumulation of fibrillar ATP particles, which would hardly intrude into the pores of the support during the dip-coating process, in contrast to their fine spherical counterparts. Hence, it is unnecessary to prepare the traditional intermediate layer for a high performance membrane (Fang *et al.* 2011). In addition, irregular accumulation of particles is conducive to obtaining an active layer with high porosity and tortuosity, which is prone to remove contaminants in the wastewater efficiently (De Angelis & de Cortalezzi 2013). According to Figure 5(c), the active layer can be clearly distinguished from the support, with an approximate thickness of 40 μm from a cross-sectional view.

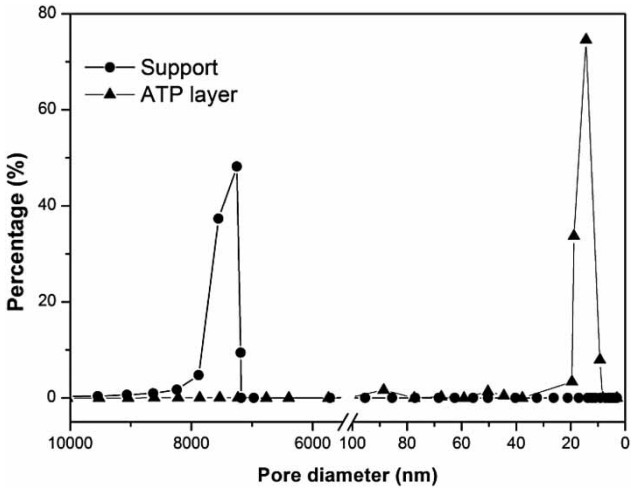


**Figure 4** | Pore size distribution of the support and ATP membrane.

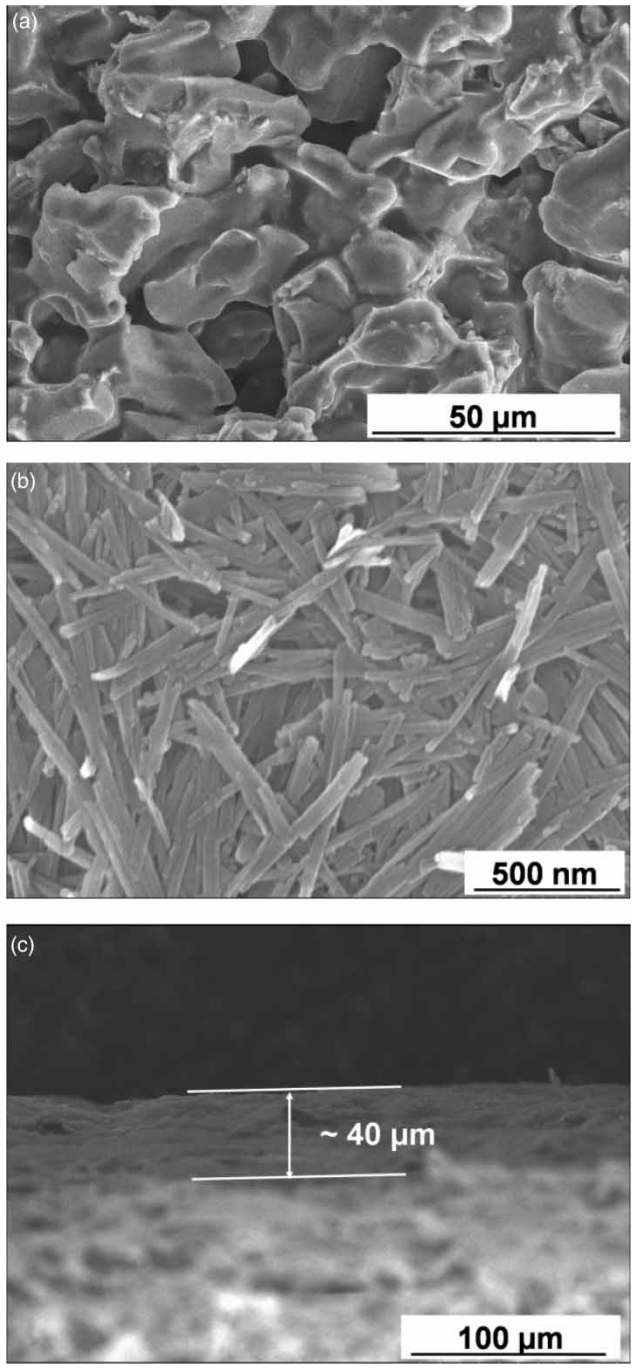


**Figure 5** | SEM images of $Al_2O_3$ substrate (a), ATP layer (b) and cross section (c).

## Rejection performance of ATM for synthetic CBW (laboratory scale)

Before developing the module based on the ATM, it is of primary importance to collect the hydraulic data for the ATM

in the laboratory. To evaluate the membrane permeability under dead-end mode, DI water was subjected to permeation under different operating pressures as shown in Figure 6. It is observed that the ATM exhibits an almost linear relationship between flux and trans-membrane pressure (TMP) with a permeability of 1,411.87 L $m^{-2}$ $h^{-1}$ $MPa^{-1}$ at pH 6.36 and a temperature of 27 °C. It is noteworthy that the permeability of the ATM is relatively lower than that of reported values with similar pore size distributions (Llanos *et al.* 2010; Xu *et al.* 2010; Muthukumaran & Baskaran 2014). This may be ascribed to the thick active layer as shown in Figure 5(c), which can increase the intrinsic membrane resistance of the ATM inextricably, and subsequently lead to a decline in permeability.

Furthermore, according to the practical operation of the WNS20-1.57YQ boiler, the outlet pressure of the CBW maintained at 0.14 ± 0.01 MPa after decompression and expansion through an expansion tank. Thus, except for special indications, the driving pressure for dead-end filtration is 0.14 MPa in this work. Figure 7 presents the hydraulic performance of the ATM for treating the single salt solution. As can be observed from Figure 7(a) and 7(b), water flux for each model solution deteriorates gradually as the ion concentration increases. In terms of ion retention, the rejection of $CO_3^{2-}$ seems to be maintained at a high level (~91%) throughout the concentration range based on Figure 7(a). Also, the rejection of $SO_4^{2-}$ has an increasing trend from the initial concentration and finally stays stable at about 92% according to Figure 7(b).

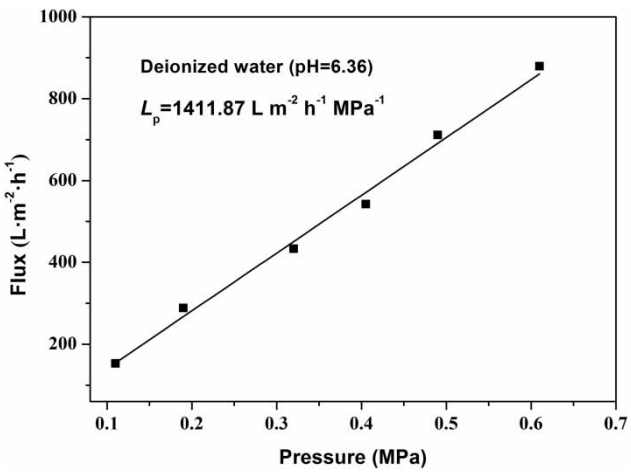


**Figure 6** | Variation of pure water flux as a function of driving pressure.

Based on the data of the hydrated ionic radius, a preliminary judgment can be made that the rejection mechanism of the ATM for target ions could hardly be the physical sieve effect: the hydrated radius of $SO_4^{2-}$ and $CO_3^{2-}$ are 0.300 nm and 0.394 nm, respectively (Tansel *et al.* 2006), which are far smaller than the average pore size of the ATM (shown in Figure 4). Therefore, the characteristics of ion retention and water flux may be attributed to the surface electrical properties of the ATM, such as Donnan exclusion, dielectric effect and Coulomb repulsion. In addition, feed solutions in this study were prepared through sodium carbonate ($Na_2CO_3$) and sodium sulfate ($Na_2SO_4$). Hence, $Na^+$ has a noticeable reserve in each feed, which can aggravate the flux of nano-scale membranes and generate a decreasing tendency with the increase in ion concentration (Kaewsuk *et al.* 2012).

In order to provide evidence for our assumption on the rejection mechanism and surface electrical properties of the ATM, the retention of salts ($Na_2CO_3$ and $Na_2SO_4$) at different pH values were conducted as shown in Figure 8. The concentrations of two ion species were selected in reference to that in the real CBW (listed in Table 1). Moreover, given that $CO_3^{2-}$ is a radical group in the acidic medium, the degree of ionization and speciation will be affected by pH. Thus, in order to reflect real ion retention of $CO_3^{2-}$, the initial testing pH value was selected at eight for the rejection process. Figure 8 reveals that the ATM exhibits a pH-sensitive property for ion retention. It may be concluded that ion retention versus pH curves are the signature of a charged membrane that rejects ions principally by electrostatic interactions (Luo & Wan 2013). The zeta potential of the ATM provides further direct evidence for surface electrical properties of the ATM as shown in Figure 9. It is worth further attention that an indifferent electrolyte (NaCl) was used as the test medium in order to avoid a potential shift caused by the adsorption of asymmetric salts ($Na_2SO_4$ and $Na_2CO_3$). According to Figure 9, the ATM shows amphoteric behavior with an isoelectric point (IEP) at about pH 5.0, which is almost in line with the results obtained from Figure 8. The small deviation may result from the adsorption of divalent anions, which subsequently results in the early charge inversion of the membrane surface.

According to Figure 8, for sulfate, ion retention seems to be inefficient in the low pH range (less than 4.9);

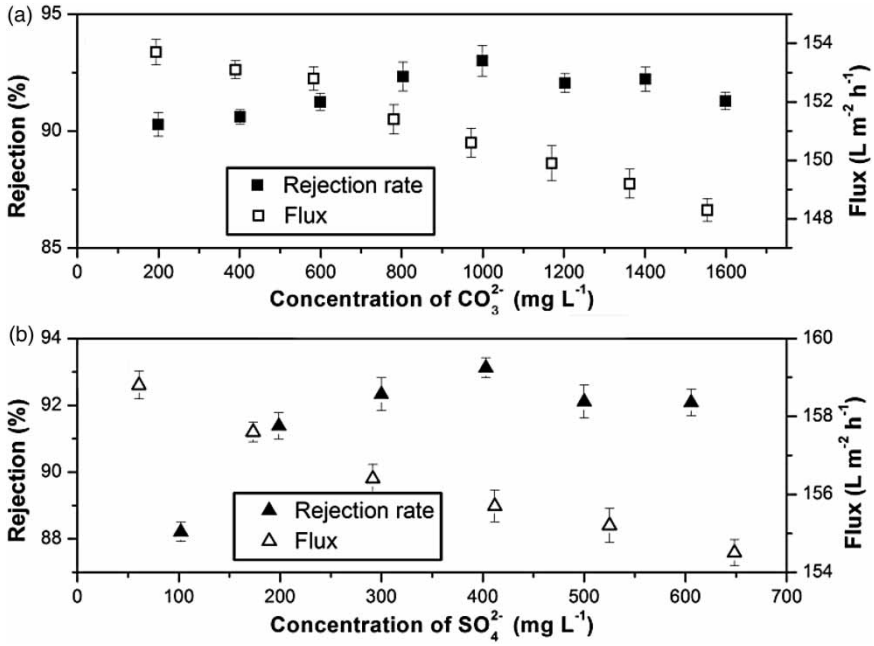


**Figure 7** | Rejection performance of the ATP for a single electrolyte solution at 27 °C: (a) sodium carbonate; (b) sodium sulfate.

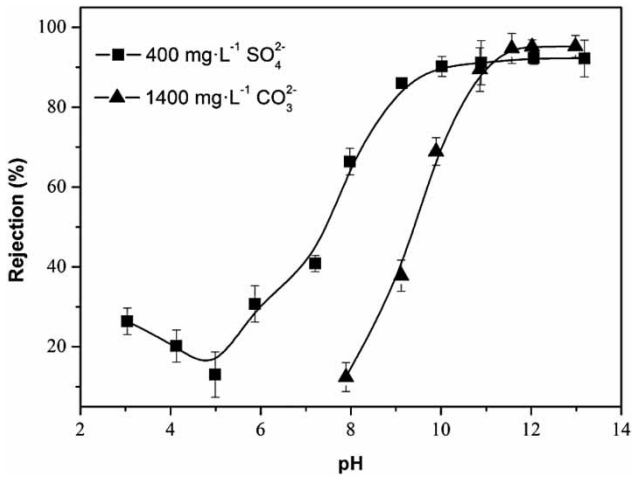


**Figure 8** | Retention of $CO_3^{2-}$ and $SO_4^{2-}$ under various pH values at 27 °C.

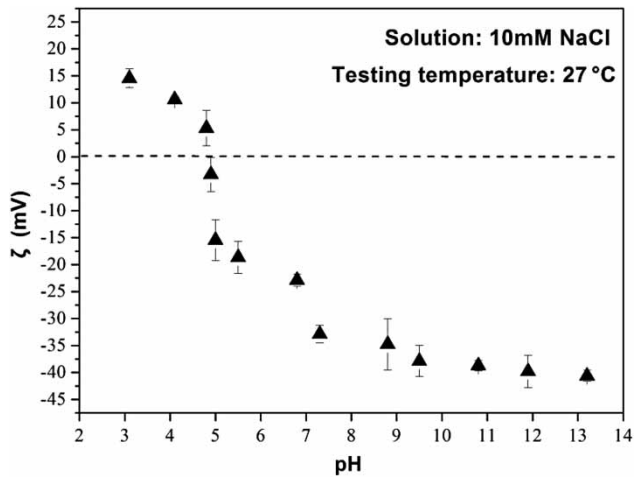


**Figure 9** | Variation of ζ potential of the ATM as a function of pH.

subsequently, the rejection rate shows an increased tendency, and finally keeps stable at around 90% as pH increases. For carbonate, the rejection rate increases with the elevated pH values, and a similar steady state appears when the pH exceeds 11. Based on conclusions made by other researchers (Van der Bruggen *et al.* 2001), the IEP of the ATM is expected to have a pH value of 4.9 for the simulated CBW.

Furthermore, allowing for the mean pore size of the ATM (12.7 nm), a little $SO_4^{2-}$ and $CO_3^{2-}$ can be directly rejected by the membrane through its surface electrical properties. Much work has indicated that the crystal lattice of ATP contained various cations ($Na^+$, $Ca^{2+}$, and $Al^{3+}$) (Deng *et al.* 2013; Dong *et al.* 2013). According to the XRD patterns shown in Figure 3, the main crystal structure of ATP was not changed drastically after sintering. Thus, it is

reasonable for cations to be still kept in the original lattice. Some cations in the lattice can exchange with $Ca^{2+}$, $Mg^{2+}$ and other cations, when the membrane contacts with polar feeds (Huang *et al.* 2007). However, this exchange process is hard for $Na^{+}$ in the lattice based on the conclusion drawn by Liu *et al.* (2013). As a result, the concentration of $Na^{+}$ in the membrane pores is lower than that in the bulk solution, and Donnan exclusion can be formed (Vezzani & Bandini 2002). For the rejection of $SO_4^{2-}$, the ATM presents a positive surface charge when the pH values were less than the IEP, because of the confined cations in the lattices. Therefore, $Na^{+}$ is rejected due to electrostatic repulsion; $SO_4^{2-}$ is also rejected for charge balance. With increasing pH, the rejection rate decreases because the membrane charge decreases as well, and reaches a minimum at a pH value corresponding to the IEP.

At pH >IEP, another mechanism may be responsible for the increasing rejection rate as the pH increases, which is depicted in Figure 10. Owing to the cations kept in the lattices of the ATM, anions in the feed can be adsorbed on the inner wall of pores through Coulomb's law. Adsorption of anions generates a negative charged surface, for which the concentration of anions in the pores of the ATM is larger than that in the bulk solution. In this case, the dielectric effect plays a key role in co-ion retention (Déon *et al.* 2009). In order to keep electrical neutrality, cations such as $Na^{+}$ are forced to stay on the feed side. Moreover, hydroxyl ions ($OH^{-}$) will enhance the dielectric effect at the pH range over 7. Therefore, the rejection rate increases gradually, since the retention of anions is vigorous by the enhanced negatively charged surface.

The rejection process towards $CO_3^{2-}$ seems to be complicated due to the special dissociation constant of carbonate.

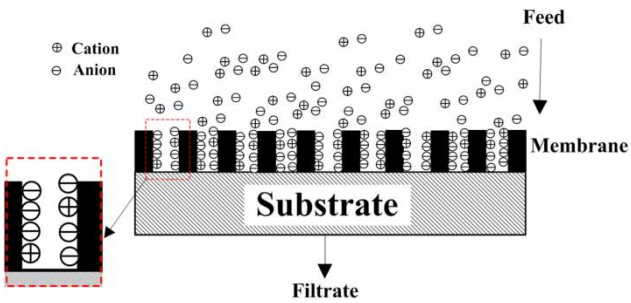


**Figure 10** | Schematic diagram of the rejection mechanism of ATM (pH>4.9).

At room temperature, monovalent ions ($HCO_3^{-}$) are dominant in the feed at pH 8 or lower (Calderón *et al.* 2008). As pH increases, $HCO_3^{-}$ will deprotonate, followed by the formation of $CO_3^{2-}$. Divalent ions can be rejected following a mechanism akin to that of sulfate mentioned above.

In general, Donnan exclusion and the dielectric effect are the essential factors to determine the retention efficiency of the ATM. In detail, Donnan exclusion is more prominent than the repulsion of the dielectric effect for sulfate retention in the pH range below the IEP. The very reverse, the dielectric effect is the main cause of increasing retention when the pH value is over the IEP. Considering the particularity of $CO_3^{2-}$, the dielectric effect might be the controlling factor during the limited ion retention.

Figure 11 shows the treatment effect towards practical CBW of the ATM. During filtration, both the samples of feed and filtrate were taken in triplicate, respectively; and the ion concentration of either $SO_4^{2-}$ or $CO_3^{2-}$ was measured to evaluate the retention efficiency. Based on Figure 11, a relatively stable rejection rate can be observed for both ions, which indicates the ATM still has the excellent separation performance for CBW. Another aspect which deserves attention is that small suspended solids and organic species in CBW also contribute to the high ion retention, because the ATM can hardly be fouled or clogged by solid impurities. The marginally downward trend of the two curves may be induced by reversible ion accumulation at the membrane vicinity. This phenomenon, normally known as concentration polarization, manifests itself as flux decline and decreased transmission over time. In this respect, however, it is prone to enhance the electroviscous effect caused by ion aggregation in narrow membrane pores. Thus, transmembrane diffusion of the target ions can be retarded, yielding high ion retention (Bowen & Yousef 2003).

## Application of ATM to the industrial boiler (field test)

Several filters based on the ATM were developed with an effective area of 0.7 $m^2$, which were mounted onto the outlet pipe of an expansion tank serving the WNS20-1.57YQ low-pressure boiler in dead-end filtration mode. The process flowchart of our field test is depicted in Figure 12. It is noteworthy that alkalinity is usually used as a substitute for the concentration of $CO_3^{2-}$, $OH^{-}$ and $HCO_3^{-}$.

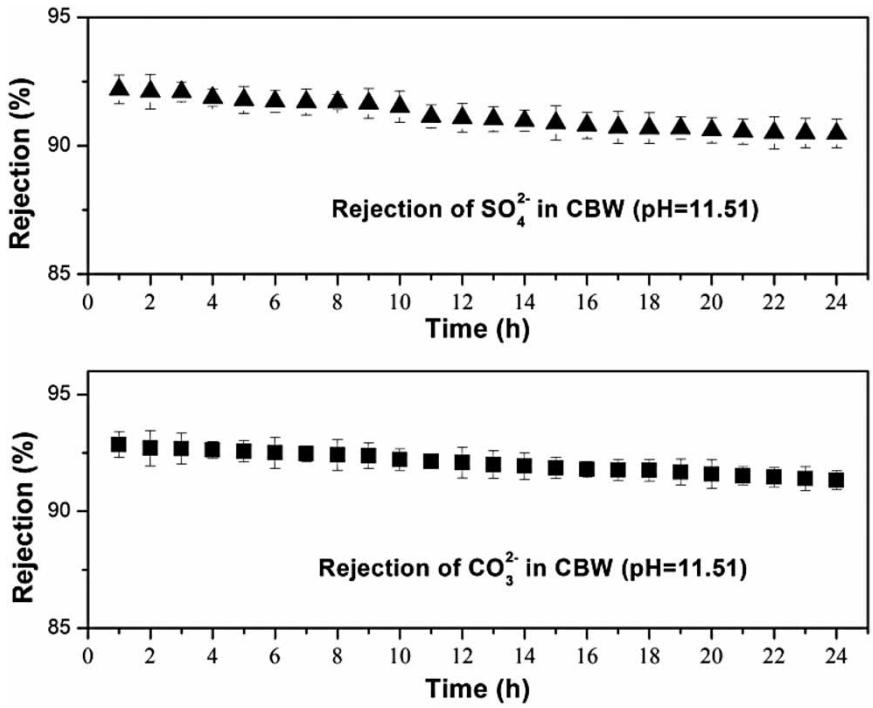


**Figure 11** | Treatment of CBW from the industrial boiler by ATM at 27 °C.

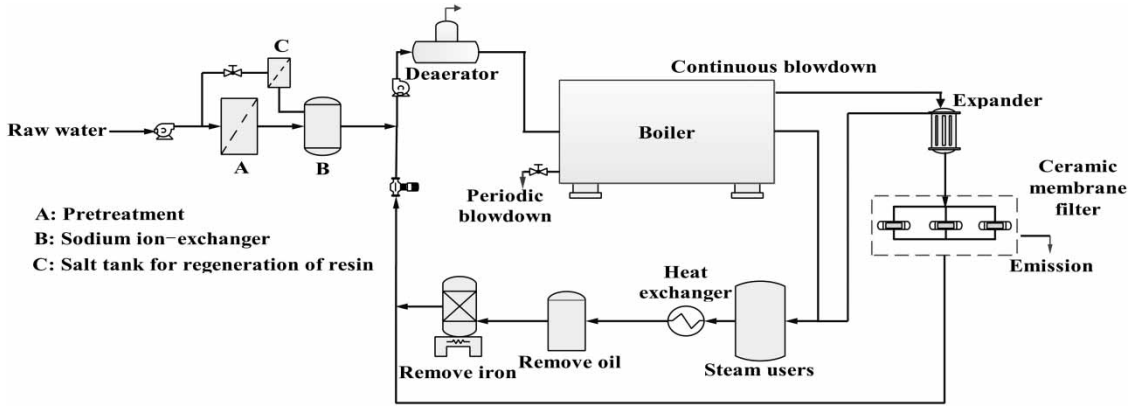


**Figure 12** | Schematic diagram of the industrial boiler water/steam system.

Table 4 lists the monitored parameters of the CBW before and after treatment. On observing the four parameters of treated water, they are all improved in different degrees. In detail, alkalinity has a substantial decrement to be maintained at an average value of 1.22 mM $L^{-1}$; whereas the pH of the treated water remained outside the required standard. This can be attributed to the insufficient rejection of monovalent anions ($OH^-$), which can keep the filtrate alkaline. In addition, the rejection of $SO_4^{2-}$ is in good agreement with the results of laboratory-scale experiments. Removal of dissolved solids in the CBW results in a pronounced decline of conductivity.

In summary, based on the prescribed National Standards (Standard GB/T1576-2008), it can be concluded that all the parameters meet the criteria of the softened water except pH value, which is limited between 7 and 9. In

**Table 4** | Water quality parameters of CBW before and after treatment

| Parameter | Unit | Before treatment | | After treatment | | National standard |
|---|---|---|---|---|---|---|
| Alkalinity | mM $L^{-1}$ | Max. 17.52 Min. 11.50 | Mean 13.28 | Max. 1.99 Min. 0.98 | Mean 1.22 | 6–24 |
| pH | – | Max. 11.87 Min. 11.23 | Mean 11.49 | Max. 9.33 Min. 8.87 | Mean 9.06 | 7–9 |
| $SO_4^{2-}$ | mg $L^{-1}$ | Max. 419.88 Min. 391.29 | Mean 407.11 | Max. 38.16 Min. 25.36 | Mean 27.52 | 10–30 |
| Conductivity | μS $cm^{-1}$ 27 °C | Max. 3,860.09 Min. 3,440.00 | Mean 3,580.15 | Max. 522.83 Min. 507.24 | Mean 515.22 | ≤550 |

order to make the pH value be appropriate to the standard, the demineralizer system out of the boiler should be operated at a low load to supply a small amount of softened water. In this way, the filtrate treated by ATM can be used as the make-up water and pumped into the boiler after mixing with the softened water.

After the application of ATM filters, the volume of the CBW has a noticeable decrement from 1.82 to 0.37 $m^3 h^{-1}$. According to Equation (5), the evaluated blowdown rate is about 1.98%, which is far lower than the original value (about 9.7%).

Besides reusing the treated water, another aspect which should be mentioned is that the heat contained in the CBW could also be recycled along with the filtrate. In this case, recycling the treated CBW can reduce the consumption of fuels, which will have various environmental benefits.

## CONCLUSION

An $Al_2O_3$ supported ATP membrane was prepared for carbonate and sulfate removal. Based on the results of surface morphology, porosity and adhesion strength between the active layer and substrate, the sintering temperature for ATM was selected as 800 °C. The sintering process only changed the interplanar spacing rather than the crystal phase species of ATP according to the XRD analysis. The mean pore size of the ATP active layer was calculated as 12.7 nm with a thickness of about 40 μm.

Under dead-end mode, ATM exhibited a good linear relationship between pure water flux and TMP with a permeability of 1,411.87 L $m^{-2} h^{-1}$ $MPa^{-1}$ at room temperature (27 °C). The rejection performance of ATM exhibited the pH-sensitive property for carbonate and sulfate solutions with an IEP at pH 4.9. Donnan exclusion and the dielectric effect could be responsible for the high divalent ion retention: when the pH was over 11, the rejection rate could maintain at about 90%.

Several filters were developed based on ATM to purify the practical CBW from a low-pressure boiler. According to the data from the field test, the parameters of water quality after treatment were akin to that of make-up water for low-pressure boilers except for the pH values. Thus, the treated water could be reused after mixing with a defined amount of softened water, which would reduce the operational load of the demineralizer system. In sequence, the continuous blowdown rate had a substantial decrease to about 1.98%. In addition, the obtained results revealed that recycling the treated CBW could essentially be significant in saving water and energy.

## ACKNOWLEDGEMENTS

This work would not have been possible without the financial support from the National Natural Science Foundation of China (No. 31501435) and Research Initiation Funds for Young Teachers of Beijing Technology and Business University (QNJJ2015-30). The authors also thank the financial support for field tests from the Innovation Research Team of Polymeric Functional Film of Beijing Technology and Business University (No. 19008001071).

## REFERENCES

Agana, B. A., Reeve, D. & Orbell, J. D. 2013 Industrial water reclamation using polymeric membranes – case studies

involving a car manufacturer and a beverage producer. *J. Water Reuse Desal.* **3**, 357–372.

APHA/AWWA/WEF 1998 *Standard Methods for the Examination of Water and Wastewater*. 20th edn. American Public Health Association/American Water Works Association/Water Environment Federation, Washington, DC.

Bowen, W. R. & Yousef, H. N. S. 2003 Effect of salts on water viscosity in narrow membrane pores. *J. Colloid Interf. Sci.* **264**, 452–457.

Calderón, J. A., Barcia, O. E. & Mattos, O. R. 2008 Reaction model for kinetic of cobalt dissolution in carbonate/bicarbonate media. *Corros. Sci.* **50**, 2101–2109.

Chang, Q., Zhou, J.-E., Wang, Y., Liang, J., Zhang, X., Cerneaux, S., Wang, X., Zhu, Z. & Dong, Y. 2014 Application of ceramic microfiltration membrane modified by nano-$TiO_2$ coating in separation of a stable oil-in-water emulsion. *J. Membr. Sci.* **456**, 128–133.

Chibowski, E. & Holysz, L. 1992 Use of the washburn equation for surface free energy determination. *Langmuir* **8**, 710–716.

De Angelis, L. & de Cortalezzi, M. M. F. 2013 Ceramic membrane filtration of organic compounds: effect of concentration, pH, and mixtures interactions on fouling. *Sep. Purif. Technol.* **118**, 762–775.

Deng, Y., Gao, Z., Liu, B., Hu, X., Wei, Z. & Sun, C. 2013 Selective removal of lead from aqueous solutions by ethylenediamine-modified attapulgite. *Chem. Eng. J.* **223**, 91–98.

Déon, S., Dutournié, P., Limousy, L. & Bourseau, P. 2009 Transport of salt mixtures through nanofiltration membranes: numerical identification of electric and dielectric contributions. *Sep. Purif. Technol.* **69**, 225–233.

Dong, K., Qiu, F., Guo, X., Xu, J., Yang, D. & He, K. 2013 Polyurethane-attapulgite porous material: preparation, characterization, and application for dye adsorption. *J. Appl. Polym. Sci.* **129**, 1697–1706.

Fang, J., Qin, G., Wei, W. & Zhao, X. 2011 Preparation and characterization of tubular supported ceramic microfiltration membranes from fly ash. *Sep. Purif. Technol.* **80**, 585–591.

Huang, J., Liu, Y., Jin, Q., Wang, X. & Yang, J. 2007 Adsorption studies of a water soluble dye, reactive red mf-3b, using sonication-surfactant-modified attapulgite clay. *J. Hazard. Mater.* **143**, 541–548.

Jakobs, E. & Koros, W. J. 1997 Ceramic membrane characterization via the bubble point technique. *J Membr. Sci.* **124**, 149–159.

Kaewsuk, J., Lee, D. Y., Lee, T. S. & Seo, G. T. 2012 Effect of ion composition on nanofiltration rejection for desalination pretreatment. *Desalin. Water. Treat.* **43**, 260–266.

Li, J., Gan, J. & Li, X. 2009 Leaching of aluminum and iron from boiler slag generated from a typical Chinese steel plant. *J. Hazard. Mater.* **166**, 1096–1101.

Liu, W., Yao, C., Wang, M., Ji, J., Ying, L. & Fu, C. 2013 Kinetics and thermodynamics characteristics of cationic yellow X-GL adsorption on attapulgite/rice hull-based activated carbon nanocomposites. *Environ. Prog. Sustain Energy* **32**, 655–662.

Liu, W., Yang, T., Xu, J., Chen, Q., Yao, C., Zuo, S., Kong, Y. & Fu, C. 2015 Preparation and adsorption property of attapulgite/carbon nanocomposite. *Environ. Prog. Sustain. Energy* **34**, 437–444.

Llanos, J., Williams, P. M., Cheng, S., Rogers, D., Wright, C., Pérez, Á. & Cañizares, P. 2010 Characterization of a ceramic ultrafiltration membrane in different operational states after its use in a heavy-metal ion removal process. *Water Res.* **44**, 3522–3530.

Luo, J. Q. & Wan, Y. 2013 Effects of pH and salt on nanofiltration – a critical review. *J. Membr. Sci.* **438**, 18–28.

Luo, F., Dong, B., Xie, J. & Jiang, S. 2012 Scaling tendency of boiler feedwater without desiliconization treatment. *Desalination* **302**, 50–54.

Maarten Biesheuvel, P. & Verweij, H. 1999 Design of ceramic membrane supports: permeability, tensile strength and stress. *J. Membr. Sci.* **156**, 141–152.

Muthukumaran, S. & Baskaran, K. 2014 Comparison of the performance of ceramic microfiltration and ultrafiltration membranes in the reclamation and reuse of secondary wastewater. *Desalin. Water Treat.* **52**, 670–677.

Rana, D. & Matsuura, T. 2010 Surface modifications for antifouling membranes. *Chem. Rev.* **110**, 2448–2471.

Rodemann, K. & Staude, E. 1995 Electrokinetic characterization of porous membranes made from epoxidized polysulfone. *J. Membr. Sci.* **104**, 147–155.

Saidur, R. 2011 Energy savings and emission reductions in industrial boilers. *Therm. Sci.* **15**, 705–719.

Shi, W. X., Duan, Y. S., Yi, X. S., Wang, S., Sun, N. & Ma, C. 2013 Biological removal of nitrogen by a membrane bioreactor-attapulgite clay system in treating polluted water. *Desalination* **317**, 41–47.

Shirazi, M. M. A., Kargari, A., Bazgir, S., Tabatabaei, M., Shirazi, M. J. A., Abdullah, M. S., Matsuura, T. & Ismail, A. F. 2013 Characterization of electrospun polystyrene membrane for treatment of biodiesel's water-washing effluent using atomic force microscopy. *Desalination* **329**, 1–8.

Standard GB/T 1576-2008 *Water Quality for Industrial Boilers*. General Administration of Quality Supervision, Inspection and Quarantine of China, Standardization Administration, China.

Standard GB/T 6907-2005 *Analysis of Water Used in Boil and Cooling System – The Sampling Method of Water*. General Administration of Quality Supervision, Inspection and Quarantine, Standardization Administration, China.

Standard GB/T 9286-1998 *Paints and Varnishes – Cross Cut Test for Films*. General Administration of Quality Supervision, Inspection and Quarantine, China.

Tansel, B., Sager, J., Rector, T., Garland, J., Strayer, R. F., Levine, L., Roberts, M., Hummerick, M. & Bauer, J. 2006 Significance of hydrated radius and hydration shells on ionic permeability during nanofiltration in dead end and cross flow modes. *Sep. Puri. Technol.* **51**, 40–47.

Van der Bruggen, B., Daems, B., Wilms, D. & Vandecasteele, C. 2001 Mechanisms of retention and flux decline for the nanofiltration of dye baths from the textile industry. *Sep. Purif. Technol.* **22–23**, 519–528.

Vezzani, D. & Bandini, S. 2002 Donnan equilibrium and dielectric exclusion for characterization of nanofiltration membranes. *Desalination* **149**, 477–483.

Wei, G., Fan, B. M., Wei, Y. P., Xu, S. S., Zhao, Z. J. & Qiao, N. 2013 Preparation of a nano-scale ceramic membrane and its application in the medium-pressure boiler with phosphate treatment. *Desalination* **322**, 167–175.

Xu, J., Chang, C. Y. & Gao, C. 2010 Performance of a ceramic ultrafiltration membrane system in pretreatment to seawater desalination. *Sep. Purif. Technol.* **75**, 165–173.

Yin, H. & Kong, M. 2014 Simultaneous removal of ammonium and phosphate from eutrophic waters using natural calcium-rich attapulgite-based versatile adsorbent. *Desalination* **351**, 128–137.

First received 11 September 2015; accepted in revised form 24 November 2015. Available online 4 January 2016